Strength degradation mechanism of iron coke prepared by mixed coal and Fe_2O_3

Chen Yin[a,b], Shuxing Qiu[a,d], Shengfu Zhang[a,b,*] , Farooq Sher[c], Hua Zhang[a,b], Jian Xu[a,b], Liangying Wen[a,b,*]

[a]College of Materials Science & Engineering, Chongqing University, Chongqing 400044, P.R. China

[b]Chongqing Key Laboratory of Vanadium-Titanium Metallurgy & Advanced Materials, Chongqing University, Chongqing 400044, P.R. China

[c]School of Mechanical, Aerospace and Automotive Engineering, Faculty of Engineering, Environment and Computing, Coventry University, Coventry CV1 5FB, UK

[d]State Key Laboratory of Vanadium and Titanium Resources Comprehensive Utilization, Panzhihua Iron & Steel Research Institute, Panzhihua 617000, P.R. China

Chen Yin, E-mail: yinchen@cqu.edu.cn

Shuxing Qiu, E-mail: qiusx105@163.com

*Shengfu Zhang (Corresponding author), E-mail: zhangsf@cqu.edu.cn

Farooq Sher (Corresponding author), E-mail: Farooq.Sher@coventry.ac.uk

Hua Zhang, E-mail: zhanghuacqu@163.com

Jian Xu, E-mail: jxu@cqu.edu.cn

*Liangying Wen (Corresponding author), E-mail: cquwen@cqu.edu.cn

Abstract

Iron coke, as a new type of blast furnace burden is helpful for energy saving, emission reduction and green production of iron making. This study aims to investigate the strength degradation mechanism of iron coke prepared by mixed coal and Fe_2O_3 to provide a theoretical direction to improve its strength. Coking and pyrolysis experiments of mixed coal and Fe_2O_3 were carried out between 400 and 500 ℃ temperature. Gieseler plastometer and derivative thermogravimetric (DTG) showed that added Fe_2O_3 inhibited the thermoplasticity and pyrolysis process of mixed coal during coking. X-ray diffraction (XRD) and Fourier transform infrared spectroscopy (FT-IR) results showed that added Fe_2O_3 decreased the aromaticity and average stacking height, but increased the interlayer spacing of crystallite, aliphatic chain length and hydrocarbon-generating potential of mixed coal during coking. Further, gas chromatography-mass spectrometer (GC-MS) analysis suggested that the added Fe_2O_3 inhibited the cleavage of C_{al}-O, C_{al}-S, C_{al}-N, C_{al}-C_{ar} and C_{al}-C_{al} bonds, reduced the generation of ethylbenzene, o-xylene and unbranched alkanes with carbon atoms in 24-26, thus decreased the amount of fluid phase generated in coking and ultimately degraded the strength of iron coke.

Keywords: Iron coke, Strength degradation, Thermoplastic behavior, Structure transformation, Pyrolysis.

1. Introduction

With a rapid increase in environmental protection pressure, steel companies are eagerly looking for new technologies that are conducive for green production. Coke could be an indispensable burden for blast furnace ironmaking. Therefore, it has been studied that improving its reactivity is helpful to accelerate the indirect reduction rate of iron ore, and to increase the reaction efficiency of blast furnace, thereby realize energy saving and consumption reduction in the process of ironmaking [1, 2]. Iron, as a transition group metal, can reduce the energy barrier formed by unstable activated complexes, promote the formation of carbon-oxygen complexes, and attract CO in the carbon-oxygen complexes through the reduction of iron oxides during gasification process to accelerate the gasification [3]. In addition, as the final product of blast furnace ironmaking, iron has no adverse effect on the blast furnace. Therefore, the use of iron-based additives to improve coke reactivity has obvious advantages [4-7].

Many studies show that [8-17] iron-containing substances are harmful to the strength of iron coke while catalyzing its reactivity, especially to the index of coke strength after reaction (CSR). As a result, the role of iron coke in the blast furnace is weakened, which is not conducive to its application in the blast furnace. It is well known that the strength of coke is closely related to the behavior of the fluid phase (metaplast) during coal pyrolysis, which determines the fluidity of coal during the thermoplastic stage. At present, fluidity and swelling are commonly used to represent the thermoplasticity of coal. The better the fluidity of coal, the lower the reactivity and the higher the CSR [18]. Studies found that the fluidity of coal in thermoplastic stage has a

parabolic relationship with the coke reactivity index (CRI) and CSR, and the CRI reaches its maximum when the fluidity is around 100 ddpm, and CRI reached to a minimum value when the fluidity is around 200 ddpm, while the change of CSR is opposite [19, 20]. Khan *et al*. [21] studied the swelling and thermoplasticity changes of coal with added Fe_2O_3 and Fe_3O_4 and verified that iron oxides is harmful to the fluidity of coal. Moreover, Fe_2O_3 has a more obvious deterioration effect on the thermoplasticity of coal than other iron minerals [21]. Through co-pyrolysis experiment of coal and Fe_2O_3, Uchida *et al*. [22] found that Fe_2O_3 reduced the thermoplasticity of coal while accompanied by its own reduction. However, it is worth noting that the above studies are based on the characteristics of the fluidity change of coal in the thermoplastic stage after adding iron-containing substance. There are only a few studies on the components of fluid phase. Therefore, it is important to understand the composition and structural transformation of mixed coal with Fe_2O_3 in the thermoplastic stage of coking [23-25].

In the present study, high reactivity iron coke was successfully prepared from mixed coal and Fe_2O_3, and its strength deterioration behavior was obtained. Further, through pyrolysis experiments and some chemical and physical tests, changes in the thermoplasticity and structural transformation of mixed coal during thermoplastic stage after adding Fe_2O_3 were compared and analyzed. Finally, the mechanism of iron coke strength degradation was established. In fact, the experimental results have guiding significance for the development of the fabrication process of iron coke.

2. Experimental

2.1 Sample preparation

Four coals (Coal-A, Coal-B, Coal-C, and Coal-D received from a steel corporation located in Northeast of China) with 0.1-0.3 mm and 0.5-3.0 mm particle size were used in this work. The characterization data of these coal samples is described in Table 1. A standard mixed coal is composed of Coal-A (30 wt.%), Coal-B (20 wt.%), Coal-C (40 wt.%) and Coal-D (10 wt.%). In order to analyze the strength degradation mechanism of iron coke with more accurately, the mixed coal is pickled to remove minerals, and the detailed information shows in our previous work [26]. Fe_2O_3 is used as a catalyst with a particle size of less than 48 μm that is chemically pure reagent. The samples of mixed coal with Fe_2O_3 or without are named as CM-Fe_2O_3 and CM-RAW respectively, the addition amount of Fe_2O_3 is 3 wt% based on coal mass [27].

Table 1. Basic thermochemical properties of coal samples.

Samples	Proximate analysis (wt.%)				Ultimate analysis (wt.%)					R_0(%)	H/C
	M_{ad}	V_{daf}	FC_d	A_d	C_{daf}	H_{daf}	O_{daf}	N_d	S_d		
Coal-A	2.30	22.25	71.90	7.52	87.97	4.95	5.11	1.45	0.37	1.228	0.06
Coal-B	1.74	31.72	61.72	9.61	85.49	5.10	6.28	1.36	1.47	1.008	0.06
Coal-C	2.34	34.40	60.94	7.12	84.30	5.66	8.87	0.94	0.15	0.85	0.07
Coal-D	1.70	18.34	70.30	13.92	88.80	4.51	5.23	1.25	1.06	1.713	0.05

M: moisture. *V*: volatile matter. *FC*: fixed carbon. *A*: ash. ad: air dried basis. d: dried basis. daf: dried and ash-free basis. R_0: the maximum reflectance of vitrinite. H/C: the ratio of element H to C.

2.2 Iron coke preparation

Iron coke was prepared in a 2 kg laboratory coke oven. The sample (CM-RAW or CM-Fe_2O_3) with a particle of 0.5-3 mm and a weight of 2 kg was loaded into a coking tank together with 10% moisture and 0.85 t/m^3 bulk density. The details of this process have been described in our previous work [27]. After coke was quenched by nitrogen, the mechanical strength and thermal properties including the abrasion resistance index

(M_{10}), drop shatter index (M_{25}), *CRI* and *CSR* were measured [27] to understand the effect of Fe_2O_3 on coke strength degradation.

2.3 Thermoplasticity analysis

Gieseler plastometer (ZKJSLDD-4C) was used to observe changes in thermoplasticity of mixed coal during coking after adding Fe_2O_3. The sample (CM-Fe_2O_3 or CM-RAW) with a particle of 0.1-0.3 mm and weight 5.0 ± 0.1 g was placed in a steel crucible fitted with four metal stirring blades at the bottom. Then the steel crucible was placed in a liquid metal bath at 300°C, and the temperature was raised to 550°C at a rate of 3°C/min. During this process, the metal stirring paddles were turned at a constant torque. When rotation speed reached to 1 ddpm, temperature and rotation degree were recorded every 1 min until the stirring paddle was no longer rotating (rotation speed <1 ddpm). So, the Gieseler fluidity curve of samples could be obtained.

2.4 Thermal behavior analysis

Thermogravimetric analyzer (STA 449F3, NETZSCH) was used to analyze the changes in pyrolysis behavior of mixed coal after adding Fe_2O_3. About 7 ± 2 mg sample (CM-Fe_2O_3 or CM-RAW) with a particle of 0.1-0.3 mm was heated from room temperature to 1050°C at a heating rate of 10°C/min under high purity of nitrogen gas with a flow rate of 50 mL/min. Thus, the change of samples weight with temperature was obtained, further the derivative thermogravimetric (DTG) curve of samples was derived.

2.5 Pyrolysis experiment

In order to study the changes in thermoplasticity and structure of mixed coal at thermoplastic stage after adding Fe_2O_3, pyrolysis experiments with different target

temperature were carried out. About 50 g sample (CM-Fe_2O_3 or CM-RAW) with a particle of 0.1-0.3 mm was put into a corundum crucible and heated from 25°C to the target temperature (400, 425, 450, 475, and 500°C) at 10°C/min under the protection of high-purity nitrogen. These target temperatures are considered to cover the temperature range of the coal thermoplastic stage [26]. Finally, the heated mixed coal was quenched to room temperature by nitrogen to obtain the required samples.

2.6 XRD analysis

The changes in carbon structure of mixed coal during thermoplastic stage after adding Fe_2O_3 were analyzed by X-ray diffractometer (MAX2500PC X, Nippon koji co. LTD). All samples were pulverized in the laboratory and screened to below 0.074 mm. The X-ray source was generated by copper $K\alpha$ radiation (40 kV, 150 mA). The scanning angular started from 15° to 90° at a rate of 4°/min, 0.02°/step. Gaussian fitting is performed on the obtained XRD spectra to obtain the required information about γ-band and π-band (002), thereby calculating the parameter f_a represents the aromaticity of mixed coal [28]. Furthermore, parameter d_{002}, and L_c represent the coal graphitization and the coal average stacking height respectively, were calculated using full width at half maximum (FWHM) and scattering angle of π-band (002) [29, 30].

2.7 FT-IR analysis

Fourier transform infrared spectroscopy (Nicolet iS5-FTIR, Thermo Fisher Scientific) was used to analyze the changes in structure transformation of functional groups of mixed coal during thermoplastic stage after adding Fe_2O_3. The sample was placed on a KBr sheet and dried under vacuum at room temperature. Each spectrum segment was scanned 32 times with a resolution of 4 cm^{-1} and the scanning wave number range was 4000-650 cm^{-1}. In addition, two characteristic parameters of CH_2/CH_3 and *A-factor* reflecting the aliphatic chain length and hydrocarbon-generating

potential of coal respectively, could be obtained by fitting the curves of two regions (3000-2800 cm^{-1} and 1700-1500 cm^{-1}) [26].

2.8 GC-MS analysis

Gas chromatography mass spectrometer (QP2010Ultra, Shimadzu) was used to analyze changes of fluid phase transformation of mixed coal during thermoplastic stage after adding Fe_2O_3. The GC-MS characteristics were described in previous studies [31] and the fluid phase can be obtained from two-step solvent extraction (first acetone, then THF) [26]. Firstly, the sample from the pyrolysis experiment were placed in acetone, and the collected extracts were named as 400-light, 425-light, 450-light, 475-light and 500-light, respectively. Then the sample was removed from acetone to THF, and the extracts collected were named as 400-heavy, 425-heavy, 450-heavy, 475-heavy and 500-heavy, respectively. Finally, the light/heavy extracts were equally divided into four parts, three of which were placed in an oven and evaporated to obtain the extract content by subtraction. The other part was refrigerated in vacuum until further analysis.

3. Results and discussion

3.1 Strength degradation of iron coke prepared by mixed coal and Fe_2O_3

As can be seen from Fig. 1, Fe_2O_3 can significantly improve the reactivity of coke with CO_2, but its degradation effect on coke strength is also very obvious. After adding Fe_2O_3, the CRI of coke increased from 36.36% to 41.57%. And the index of M_{10} and M_{25} changed from 4.94% and 94.15% to 5.78% and 92.98% respectively when Fe_2O_3 was added, which indicated that the added Fe_2O_3 would degrade the abrasion resistance index and also drop shatter index of coke. The deterioration was more obvious in the

coke strength after reaction (*CSR*). The addition of Fe_2O_3 reduced *CSR* from 61.94% to 42.78%. These results are consistent with the previous studies [8-17].

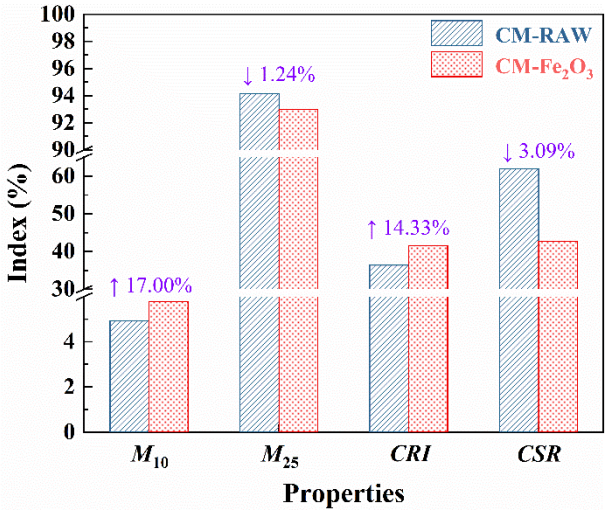

Fig. 1. Changes in coke properties after adding Fe_2O_3.

3.2 Changes in the thermoplasticity of mixed coal after adding Fe_2O_3

As shown in Fig. 2, the CM-RAW begin to soften at 422°C and then the fluidity increased with increasing temperature resulting in maximum fluidity of 195 ddpm at 455°C, after which the fluidity decreased with increasing temperature and solidified again at 491°C. The curve is convex with a thermoplastic range of 69°C. The physical changes of mixed coal during thermoplastic stage depend on the chemical changes in its molecular structure, involving the rearrangement of carbon molecules to form a fluid phase and solidification of fluid phase into low temperature graphitized carbon material (semi-coke) [32]. The thermoplastic characteristics of CM-Fe_2O_3 are similar to those of CM-RAW. Its softening temperature is 4°C higher than CM-RAW, and the solidification temperature is 2°C lower than CM-RAW. Moreover, the maximum fluidity and thermoplastic range of CM-Fe_2O_3 were reduced by 40 ddpm and 6°C compared with CM-RAW, respectively. Despite the dilution effect of Fe_2O_3 on thermoplasticity of

mixed coal, the actual plasticity range and maximum fluidity value of CM-Fe_2O_3 may be slightly larger than the measured value. However, the dilution effect of Fe_2O_3 is negligible because Fe_2O_3 is added in a small amount (3%), and the volume of two samples in the crucible does not change significantly. Therefore, the added Fe_2O_3 will reduce the thermoplasticity of coal during coking.

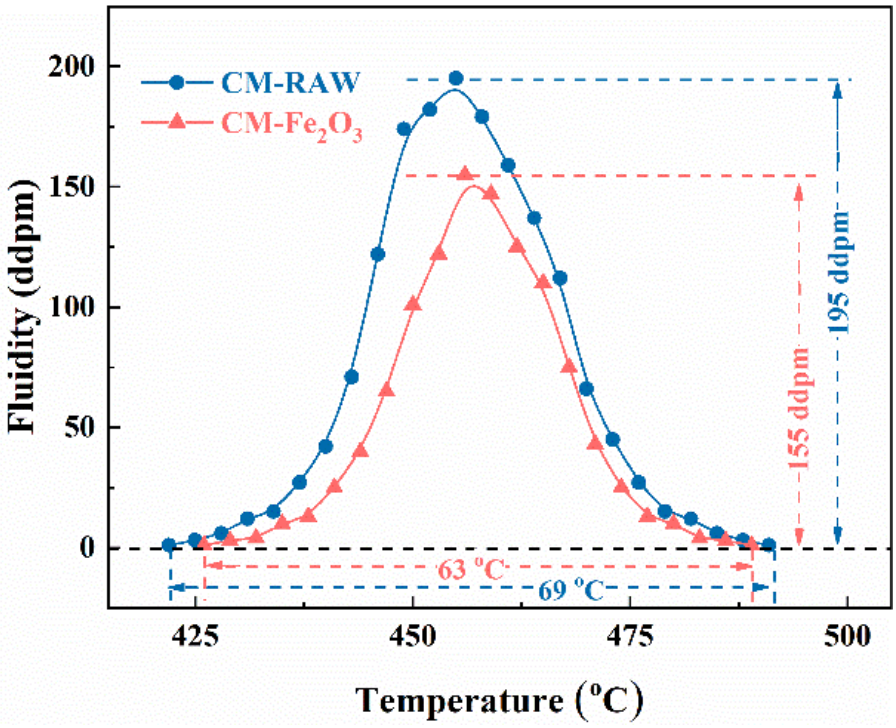

Fig. 2. Gieseler fluidity curves of mixed coal samples.

3.3. Changes in the pyrolysis behavior of mixed coal after adding Fe_2O_3

Fig. 3 provides DTG curves of mixed coal. According Fig. 3(a), the maximum weight loss rate of CM-RAW corresponds to a temperature of 471°C, which is close to the temperature of maximum fluidity. The maximum weight loss rate of CM-Fe_2O_3 is 0.137% min^{-1}, which is 0.002% min^{-1} less than CM-RAW. The results also show that the Fe_2O_3 added inhibits the pyrolysis process of mixed coal during thermoplastic stage.

According to the order of covalent bond breaking, the coking process is divided

into multiple stages as shown in Table 2 [33-42]. The peak-differentiating and imitating of DTG curve is performed to obtain the relevant information about the above bonds. It can be seen that after addition of Fe_2O_3, the content of first type bond (C_{al}-O, C_{al}-S, and C_{al}-N) decreased by 0.01, the content of second type bond (C_{al}-C_{al}) decreased by 0.94, and the content of third type bond (C_{al}-C_{ar}) decreased by 0.13. It indicated that the added Fe_2O_3 inhibits the breaking of C_{al}-C_{al}, C_{al}-C_{ar}, C_{al}-O, C_{al}-S, and C_{al}-N, which is not conducive to the decomposition of macromolecules.

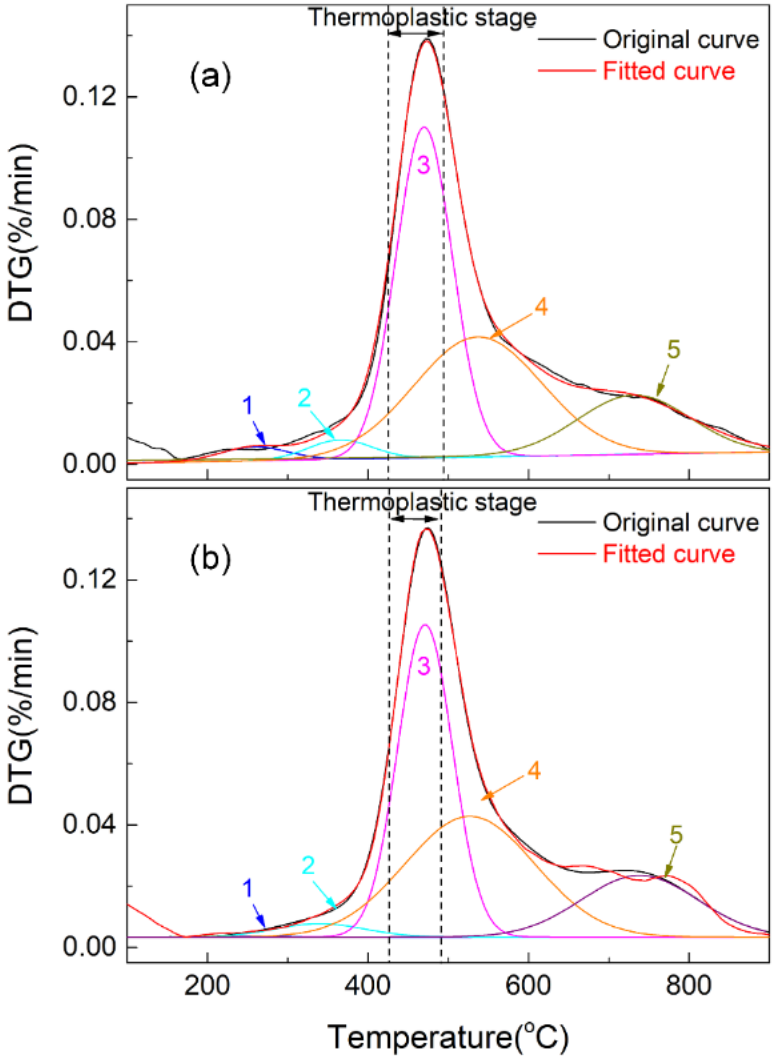

Fig. 3 DTG curves of mixed coal: (a) CM-RAW, (b) CM-Fe_2O_3.

Table 2. Bond information resulted from the curve-fitting of DTG curves of CM.

Peak	Possible origin	temperature range (°C)	CM-RAW			CM-Fe_2O_3		
			Peak temperature (°C)	Absolute area	Peak area in thermoplastic stage	Peak temperature (°C)	Absolute area	Peak area in thermoplastic stage
1[33-35]	Decomposition of carboxylic acid	<300	258.31	0.48	-	276.23	0.21	-
2[37, 38]	C_{al}-O、C_{al}-S、C_{al}-N bonds break	300-400	365.22	0.63	0.04	370.49	0.71	0.03
3[36-41]	C_{al}-C_{al} bond break	400-500	469.89	9.56	6.20	468.92	8.62	5.26
4[36-41]	C_{al}-C_{ar} bond break	500-600	536.91	7.81	1.47	526.72	7.21	1.34
5[42]	C_{ar}-H bond break	600-900	750.70	2.48	-	768.32	3.60	-

3.3 Changes in the carbon structure of mixed coal during thermoplastic stage after adding Fe_2O_3

The XRD spectra of samples is illustrated in Fig. 4. No peaks representing minerals were found in Fig. 4(a), indicating that the removal of minerals by acid treatment achieved as expected. From Fig. 4(b), the diffraction peaks of Fe_2O_3 and Fe_3O_4 could be found when CM-Fe_2O_3 was heated to 400°C and 425°C, further, the diffraction peak of Fe_2O_3 was disappeared with increasing pyrolysis temperature. It signifies that the added Fe_2O_3 gradually transforms into Fe_3O_4 in the thermoplastic stage of coking.

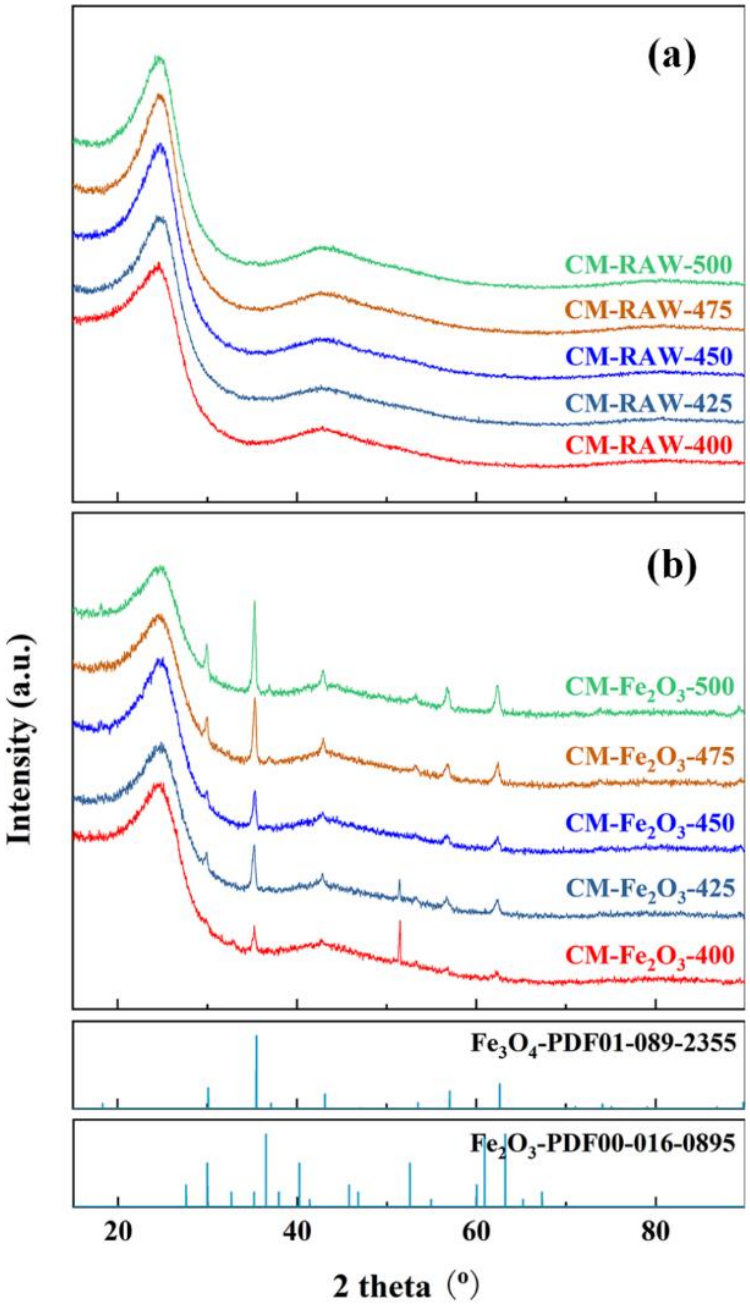

Fig. 4. XRD spectra of mixed coal in the thermoplastic stage: (a) CM-RAW, (b) CM-Fe_2O_3.

Fig. 5 shows carbon structure of mixed coal after being heated. According to Fig. 5(a), the f_a values of samples (CM-RAW, CM-Fe_2O_3) increased with an increase in temperature, indicating that the aromaticity of mixed coal increases in thermoplastic stage during coking. This may be due to: (a) the alkyl group is decomposed and removed from mixed coal during initial softening stage; (b) some of aliphatic

hydrocarbons undergo a dehydrogenation reaction during the solidification process to form aromatic structures. However, the f_a value of CM-Fe_2O_3 decreased compared with the CM-RAW at same temperature, which means the addition of Fe_2O_3 inhibits the alkyl removal or aromatic dehydrogenation reaction. It can be seen from Fig. 5(b), as pyrolysis temperature increased, the d_{002} values of samples gradually decreased. The d_{002} value of CM-Fe_2O_3 is larger than CM-RAW at same temperature, indicating that the added Fe_2O_3 inhibits the graphitization of mixed coal in thermoplastic stage. As shown in Fig. 5(c), the values of L_c increased with an increase in temperature. Furthermore, L_c value of CM-Fe_2O_3 is smaller than CM-RAW at same temperature, demonstrating that the added Fe_2O_3 reduces the average stacking height of mixed coal. Previous study [43] has confirmed that an increase in aromatic clusters helps to accommodate more free radicals. Therefore, the added Fe_2O_3 could reduce the average stacking height of coal and form less free radicals during coking, which lead to a decrease in the thermoplasticity of mixed coal.

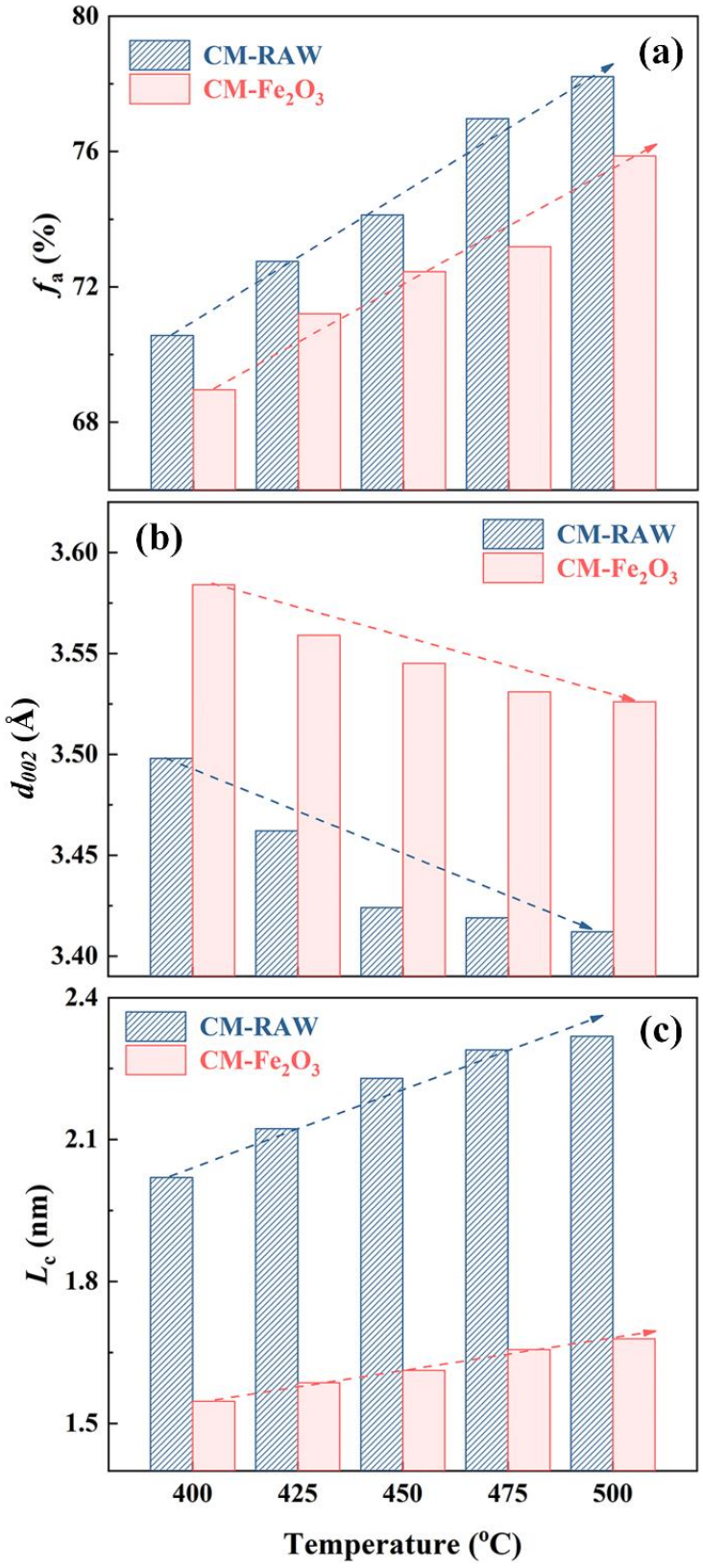

Fig. 5. Structural parameters of mixed coal in thermoplastic stage obtained from XRD spectra: (a) CM-f_a, (b) CM-d_{002}, (c) CM-L_c.

3.4. Changes in the structure of functional groups of mixed coal during thermoplastic stage after adding Fe_2O_3

The FT-IR spectra of mixed coal after heating is illustrated in Fig. 6. The spectra show that with an increase in temperature, two vibration peaks representing aliphatic C-H stretching vibrations in the range of 3000-2800 cm^{-1} have weakened. It indicates that the large aliphatic compounds of mixed coal are gradually decomposed during pyrolysis process. Moreover, the strength of vibration peak representing C=O and aromatic C=C stretching vibrations in the range of 1700-1500 cm^{-1} is also decreased with an increase in temperature. In addition, the vibration peaks of aromatic ether C-O-C and ester O=C-O-C appearing in the range of 1350-1250 cm^{-1} are weaker with increasing temperature, indicating that the mixed coal in thermoplastic stage contains a small amount of aromatic ethers and esters. Moreover, many peaks in the range of 950-750 cm^{-1} are caused by the out-of-plane deformation of C-H aromatics.

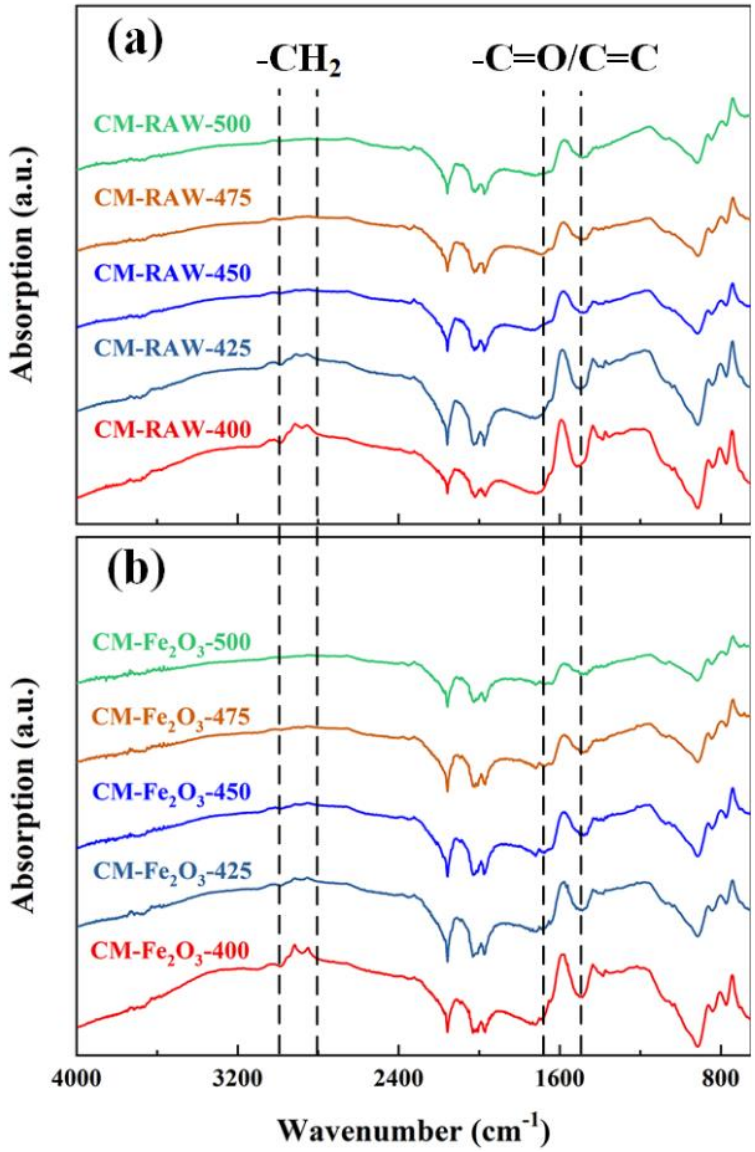

Fig. 6. FT-IR spectra of mixed coal in the thermoplastic stage: (a) CM-RAW, (b) CM-Fe_2O_3.

Fig. 7 is obtained by fitting the 3000-2800 cm^{-1} and 1700-1500 cm^{-1} regions of Fig. 6. In Fig. 7(a), the CH_2/CH_3 values of samples (CM-RAW, CM-Fe_2O_3) decreased first, and then increased with increasing temperatures, indicating that the aliphatic chain length of samples first decreases and then grow during coking. However, the addition of Fe_2O_3 improved the CH_2/CH_3 value at same temperature. This is attributed to Fe_2O_3 inhibits the breaking of certain chemical bonds of mixed coal during pyrolysis, such as methylene bridges, chemical bonds connecting aromatic rings to aliphatic side

chain, and chemical bonds connecting small molecules to aliphatic [44]. As shown in Fig. 7(b), the change of *A*-factor value of samples is the reverse of CH_2/CH_3 value. The *A*-factor value of CM-RAW first raised in the temperature range of 400-450°C and then decreased, which indicates that hydrocarbon-generating potential of CM-RAW increases, and then decreases during coking. As expected, the *A*-factor value of CM-Fe_2O_3 is larger than CM-RAW, indicating that the hydrocarbon-generating potential of mixed coal increases with the addition of Fe_2O_3. A previous study [45] has confirmed that the aliphatic hydrocarbon linked to the macromolecular structure plays an important role in the thermoplasticity of coal. In this study, the added Fe_2O_3 inhibited the decomposition of C_{al}-C_{al}, C_{al}-C_{ar}, C_{al}-O, C_{al}-S, and C_{al}-N during coking, resulting in the increase of CH_2/CH_3 and *A*-factor of mixed coal, which ultimately decreases the thermoplasticity of mixed coal.

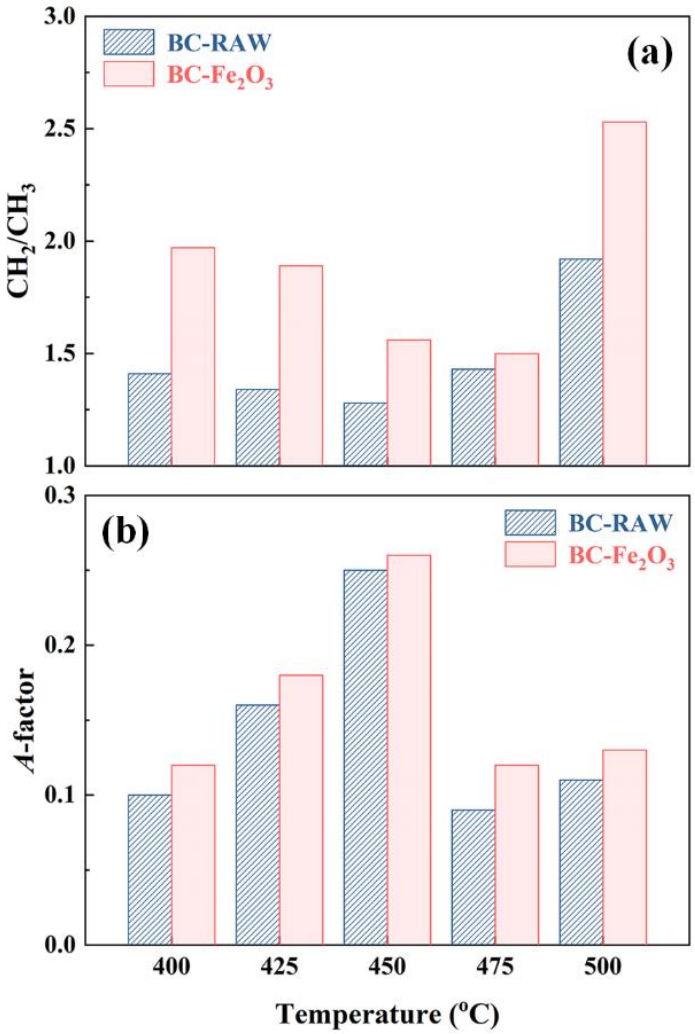

Fig. 7. Structure parameters of mixed coal in the thermoplastic stage: (a) CM-CH_2/CH_3, (b) CM-*A-factor*.

3.5. Changes in the fluid phase transformation of mixed coal during thermoplastic stage after adding Fe_2O_3

It can be seen from Fig. 8 that the contents of light and heavy extract of samples (CM-RAW, CM-Fe_2O_3) both increased first and then decreased, and finally reached to the maximum at 450°C. But the heavy extract content of samples is much higher than light extract. After adding Fe_2O_3, the maximum contents of light and heavy extract of mixed coal is 1.90% and 8.27%, respectively, which is 1.4% and 1.0% lower than CM-RAW respectively.

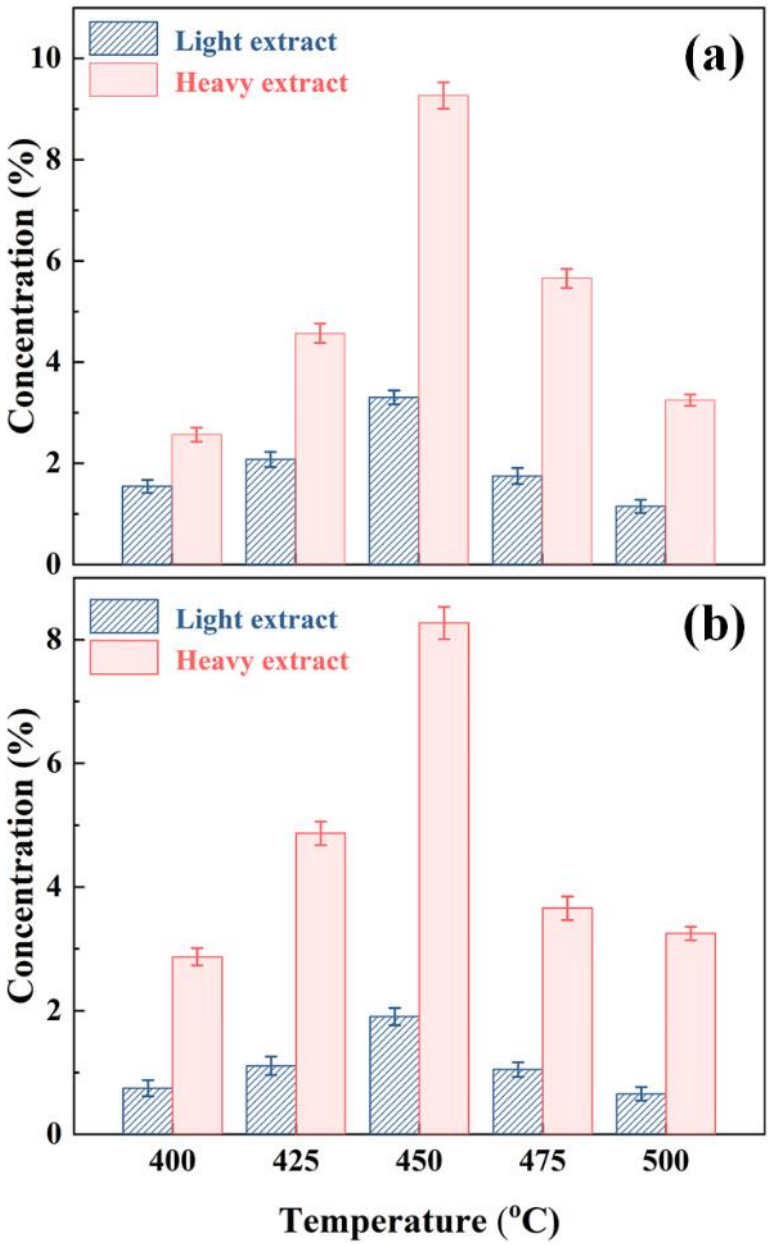

Fig. 8. Concentrations of light and heavy extract in the thermoplastic stage: (a) CM-RAW, (b) CM-Fe_2O_3.

Fig. 9 shows GC-MS chromatograms of samples extracts (CM-RAW, CM-Fe_2O_3). The detailed compounds information is shown in Table 3, Table 4, Table 5 and Table 6. According to the previous study [26], it can be seen from Fig. 9(a) and Table 3 that the components of the light extract of heated mixed coal in the thermoplastic stage are mainly included methylbenzene, ethylbenzene, o-xylene, 4-hydroxybutyric acid and

Pantolactone, and light fluid phase is mainly composed of methylbenzene, ethylbenzene and o-xylene. It can be observed from Fig. 9(c) and Table 4 that after adding Fe_2O_3, the main substances of light extract are 2-pentanone and methylbenzene during thermoplastic stage, and the light fluid phase of mixed coal containing Fe_2O_3 is mainly consist of methylbenzene. As shown in Fig. 9(b) and Table 5, the heavy extract are mainly phenolic compounds and unbranched alkanes, such as 3- (1, 1-dimethylethyl) -4-methyl-phenol, 4-methyl-2-phenol, 2,6-bis (1,1-dimethylethyl) -p-cresol and carbon number are 19-26 unbranched alkanes. Furthermore, the heavy fluid phase is unbranched alkanes with 19-26 carbon atoms. It can be seen from Fig. 9(d) and Table 6, the heavy extract of mixed coal containing Fe_2O_3 mainly consists of phenolic compounds, alkyd compounds and unbranched alkanes, which are mainly nonadecane, docosane, and tricosane, however, the heavy fluid phase mainly consists of nonadecane, docosane, tricosane and alkyd compounds.

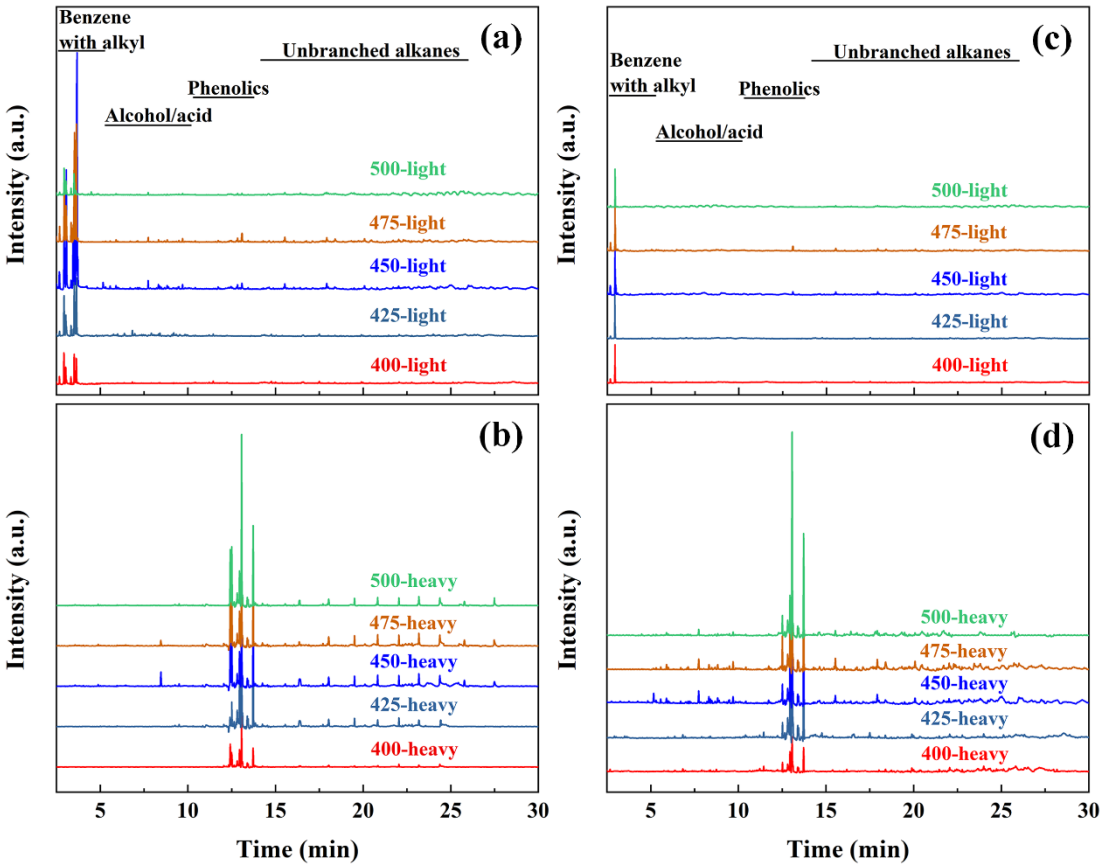

Fig. 9. GC-MS chromatograms of the extract obtained from CM in the thermoplastic stage; (a) CM-RAW light extract, (b) CM-RAW heavy extract, (c) CM-Fe_2O_3 light extract, and (d) CM-Fe_2O_3 heavy extract.

Table 3. Chemical compounds in light extract obtained from CM-RAW.

Time(min)	Compounds	Light extract of CM-RAW（%）				
		400	425	450	475	500
2.66	2-Pentanone	8.12	5.18	6.62	5.81	2.13
2.97	Methylbenzene*	16.12	19.82	21.15	18.64	15.98
3.04	Ethylbenzene *	12.15	20.22	25.33	21.15	19.67
3.33	O-xylene*	18.47	21.05	22.34	21.41	19.13
3.50	4-Hydroxybutanoic acid	29.21	21.41	11.08	13.45	15.34
3.60	Pantolactone	15.93	12.32	6.25	12.16	15.39
7.49	Pyridine	-	-	1.88	1.52	3.15
9.68	2,3-dimethyl-Dodecane	-	-	1.21	1.07	3.26
13.09	2,6-bis (1,1-dimethylethyl) -p-Cresol	-	-	2.02	2.81	3.61
15.50	Eicosane			2.12	1.98	2.34

*: light fluid phase, 400: the light extract obtained from mixed coal at the pyrolysis temperature of 400˚C.

Table 4. Chemical compounds in light extract obtained from CM-Fe_2O_3.

Time(min)	Compounds	Light extract of CM-Fe_2O_3（%）				
		400	425	450	475	500
2.66	2-Pentanone	10.23	8.46	11.52	13.34	8.21
2.97	Methylbenzene*	89.77	92.54	88.48	86.66	91.79

*: light fluid phase, 400: the light extract obtained from mixed coal at a temperature of 400°C.

Table 5. Chemical compounds in heavy extract obtained from CM-RAW.

Time(min)	Compounds	Heavy extract of CM-RAW（%）				
		400	425	450	475	500
8.56	4-hydroxy- Butanoic acid#	-	-	6.13	3.56	-
12.09	2,6-bis(1,1-dimethylethyl)-p-Benzoquinone	-	3.36	-	-	1.99
12.44	3-(1,1-dimethylethyl)-4-methyl-Phenol	16.14	9.14	14.25	15.38	17.18
12.64	4-methyl-2-Phenol	9.09	6.86	3.31	2.69	2.34
13.09	2,6-bis(1,1-dimethylethyl)-p-Cresol	56.54	33.65	17.29	17.59	29.47
13.70	2-methyl-2-(3-methyl-2-butoxyl) -Cyclohexanone	12.23	8.52	17.12	18.14	19.07
14.37	Nonadecane#	1.14	-	2.19	1.95	1.97
16.10	Docosane#	-	5.13	5.54	4.98	2.49
16.67	Tricosane #	-	3.24	3.36	2.09	1.67
18.08	Tetracosane#	-	5.34	5.61	5.12	2.57
19.51	6-methyl-Tetracosane #	-	4.28	4.01	4.68	3.29
20.79	Pentacosane#	-	4.56	4.51	4.72	2.53
22.04	3-methyl-Pentacosane #	2.53	5.88	4.95	4.19	3.27
23.18	5-ethyl-Pentacosane #	2.33	6.03	4.38	5.14	2.96
24.24	Hexacosane#	-	4.01	3.12	3.21	3.15
25.81	6-methyl-Hexacosane #			2.16	3.35	2.91
26.85	Perylene	-	-	2.07	3.21	3.14

#: heavy fluid phase compounds, 400: the heavy extract obtained from mixed coal at a temperature of 400°C.

Table 6. Chemical compounds in heavy extract obtained from CM-Fe_2O_3.

Time(min)	Compounds	Heavy extract of CM-Fe_2O_3（%）				
		400	425	450	475	500
8.56	4-hydroxy- Butanoic acid#	-	-	1.98	1.26	0.98
9.44	5-Hexene- Acetic acid#	-	-	2.02	1.62	-
11.96	2,6-bis(3,5-di-tert-butyl-4-hydroxybenzyl)-Phenol	3.24	-	3.86	3.98	2.52
12.09	2,6-bis(1,1-dimethylethyl)-p	11.01	12.98	13.01	19.34	10.59

Time(min)	Compounds	Heavy extract of CM-Fe_2O_3（%）				
		400	425	450	475	500
12.44	-Benzoquinone 3-(1,1-dimethylethyl)-4-methyl-Phenol	20.15	21.58	18.24	17.92	10.52
12.64	4-methyl-2-Phenol	9.16	10.25	7.35	6.57	8.34
13.09	2,6-bis(1,1-dimethylethyl)-p-Cresol	25.97	27.85	26.59	23.49	41.86
13.70	2-methyl-2-(3-methyl-2-butoxyl) -Cyclohexanone	20.65	18.21	17.24	16.58	20.18
14.37	Nonadecane#	3.45	3.14	2.25	4.87	2.56
16.10	Docosane#	4.21	3.19	4.27	2.19	1.38
16.67	Tricosane#	2.16	2.8	3.19	2.47	1.07

#: heavy fluid phase compounds, 400: the heavy extract obtained from mixed coal at temperature of 400°C.

Therefore, from the changes in fluid phase composition of mixed coal after adding Fe_2O_3, the main effect of Fe_2O_3 on the specific compounds during thermoplastic stage was obtained [46, 47]. Monocyclic benzene compounds (methylbenzene) are mainly generated by the reaction of decomposed complex polycyclic benzene compounds with small molecular gases. Previous work confirmed that during the pyrolysis of coal, C-C bond between benzene rings decomposed first, generating highly reactive aromatic free radicals and some small molecular gases (CH_4, H_2, and C_2H_2) [48, 49]. However, the added Fe_2O_3 inhibited these processes, as evidenced by decline of C_{al}-C_{ar} in the DTG analysis. Only methylbenzene was detected in the light extract of mixed coal after adding Fe_2O_3, while ethylbenzene and o-xylene disappeared. Therefore, it is considered that the added Fe_2O_3 inhibits the formation of ethylbenzene and o-xylene in the light fluid phase during coking. At the same time, the aliphatic side chains connected to the coal matrix are broken to generate aliphatic free radicals when mixed coal is heated. But the cleavage of C_{al}-C_{al} is inhibited by the addition of Fe_2O_3, which reduces the formation of aliphatic free radicals, thereby reducing the formation of unbranched

alkanes with 24-26 carbon atoms in the heavy fluid phase.

Fig. 10 shows changes in the fluid phase content based on the weight of mixed coal in the thermoplastic stage after adding Fe_2O_3. The relative content of light and heavy fluid phases of samples (CM-RAW, CM-Fe_2O_3) increased with an increase of temperature in the range of 400-450°C, and then decreased. Moreover, the change of heavy fluid phase is larger than that of the light fluid phase. However, the addition of Fe_2O_3 greatly reduced the content of fluid phase of mixed coal (at 450°C, the light and heavy fluid phases were reduced by 0.59% and 3.09%, respectively), resulting in the fluidity of mixed coal decreases in thermoplastic stage.

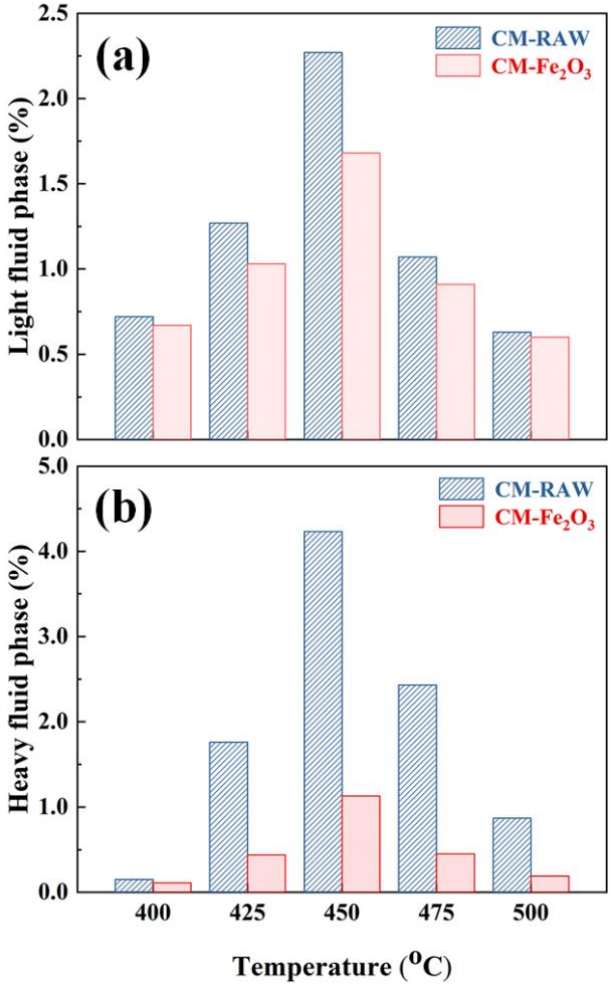

Fig. 10. The concentration of fluid phase of mixed coal in the thermoplastic stage based on the weight of mixed coal: (a) light fluid phase, and (b) heavy fluid phase.

3.6. Strength degradation mechanism of iron coke prepared by mixed coal and Fe_2O_3

As a macromolecular unit, the chemical structure of coal matrix has many chemical bonds, such as -C-C-, -CH_2-, -CH-, -O-, and -S-. which are intertwined and connected. In addition, these macromolecular units are also connected to low molecular weight substances through bond bridges. In the coking process, the depolymerization of coal mainly occurs on the side chains or bridge between the basic structural unit of coal and low molecular weight compounds, thereby generating fluid phase and a small amount of coal tar [47]. Based on our previous work [26], the components of fluid phase are mainly monocyclic benzene and long chain unbranched alkanes, and the following structural changes occur in the thermoplastic stage: (a) the formation and stabilization of fluid phase, (b) cross-linking and re-attaching of the fluid phase to coal char.

Fig. 11 shows the strength degradation mechanism of iron coke [45-50]. When the mixed coal is within the thermoplastic temperature range, the bonds of C_{al}-O, C_{al}-S, C_{al}-N, C_{al}-C_{ar}, and C_{al}-C_{al} in macromolecular units or between macromolecular units and low molecules will be broken, producing low molecular weight aromatic and aliphatic free radicals. However, when Fe_2O_3 was added, the cleavage of C_{al}-O, C_{al}-S, C_{al}-N, C_{al}-C_{ar}, and C_{al}-C_{al} was inhibited, leading to the reduction of aromatic and aliphatic free radicals. This hinders the formation of monocyclic benzene compounds (ethylbenzene and o-xylene) and linear alkanes (24-26 carbon atoms) at stage (a), leading to a decrease in the content of fluid phase, which in turn reduces the aromaticity and average stacking height, and increases the interlayer spacing, aliphatic chain length, and hydrocarbon generation potential of mixed coal. At stage (b), due to the decrease in the content of

fluid phase, hydrogen migration-acetylene addition reaction and crosslinking reaction of monocyclic benzene compounds in the fluid phase are weakened, and the formation of complex compounds is reduced. However, as the macromolecular substances of mixed coal did not decompose in the thermoplastic stage, the side group still existed in large quantities, leading to an increase in the hydrocarbon generation ability and aliphatic chain length, a decrease in the maximum fluidity and the thermoplastic stage of coal, and ultimately a reduction in coke strength.

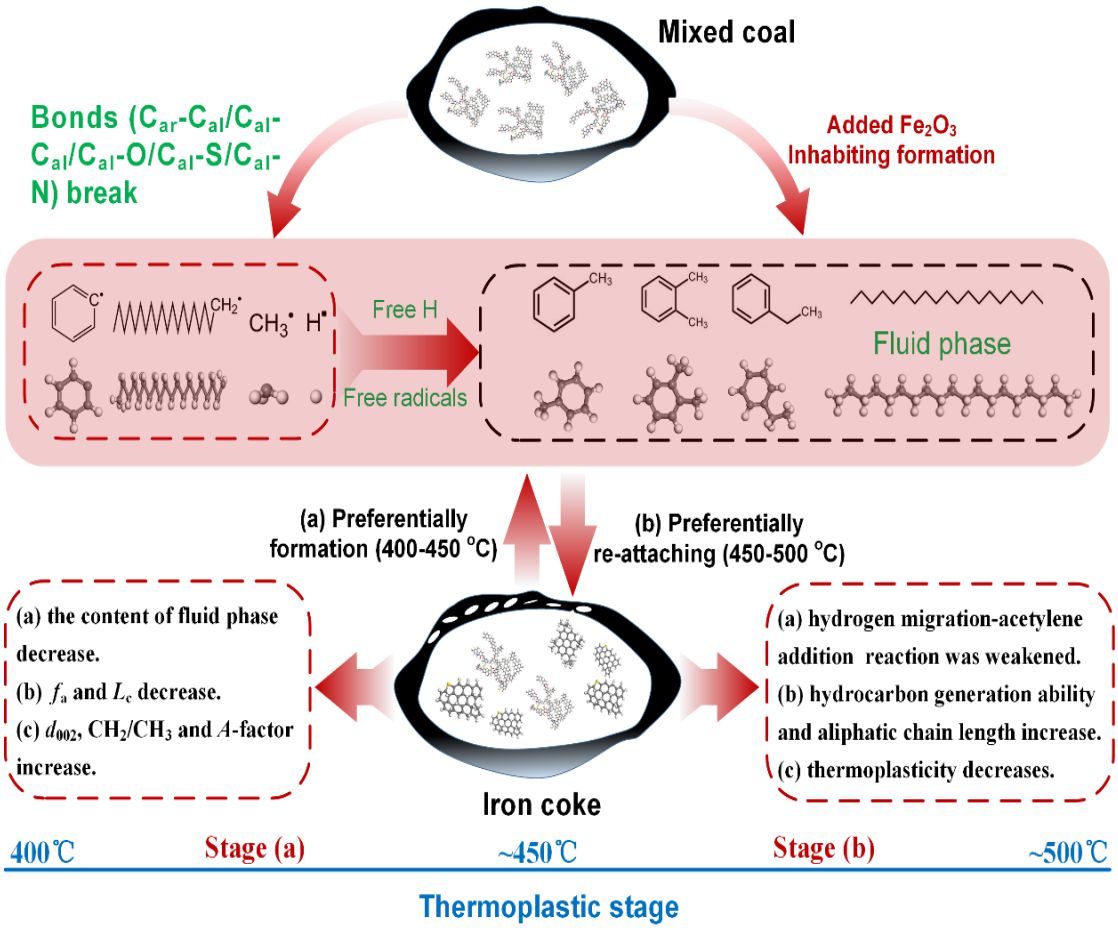

Fig. 11. Strength degradation mechanism of iron coke prepared by mixed coal and Fe_2O_3 [45-50].

4. Conclusions

This study shed light on the strength degradation mechanism of iron coke through Gieseler plastometer, TGA, XRD, FT-IR and GC-MS analysis. It was found that the addition of Fe_2O_3 hinders the cleavage of C_{al}-O, C_{al}-S, C_{al}-N, C_{al}-C_{ar} and C_{al}-C_{al}, thereby inhibiting the formation of ethylbenzene, o-xylene and unbranched alkanes with carbon atoms in 24-26, and ultimately reduces the amount of fluid phase during coking. At the same time, the inhibition of Fe_2O_3 decreases the aromaticity and average stacking height increases the interlayer spacing of the crystallite, aliphatic chain length and hydrocarbon-generating potential of mixed coal. Finally, the above changes combined to reduce the fluidity and thermoplastic range of the mixed coal after adding Fe_2O_3, resulting in the strength degradation of iron coke.

Acknowledgements

The authors thank the National Natural Science Foundation of China (Grant Nos. 51474042 & 51774061) and the Fundamental Research Funds for Central Universities (Grant No. 106112017CDJQJ138801) for financial support.

References

[1] D.M. Kundrat, T. Miwa, A. Rist, Injections in the iron blast furnace: a graphics study by means of the rist operating diagram, Metallurgical Transactions B-Process Metallurgy, 22 (1991) 363-383. https://doi.org/10.1007/bf02651235.

[2] T. Ariyama, R. Murai, J. Ishii, M. Sato, Reduction of CO_2 emissions from integrated steel works and its subjects for a future study, Isij International, 45 (2005) 1371-1378. https://doi.org/10.2355/isijinternational.45.1371.

[3]K.C. Xie, Structure and reactivity of coal, Springer, Berlin, Heidelberg, 2015. https://doi.org/10.1007/978-3-662-47337-5.

[4] Y. Ohtsuka, Y. Kuroda, Y. Tamai, A. Tomita, Chemical form of iron catalysts during the CO_2-gasification of carbon, Fuel, 65 (1986) 1476-1478. https://doi.org/10.1016/0016-2361(86)90128-6.

[5] K. Miura, K. Hashimoto, P.L. Silveston, Factors affecting the reactivity of coal chars during gasification, and indexes representing reactivity, Fuel, 68 (1989) 1461-1475. https://doi.org/10.1016/0016-2361(89)90046-x.

[6] D. Cazorlaamoros, A. Linaressolano, C.S. Delecea, Carbon gasification catalyzed by calcium - a high-vacuum temperature programmed desorption study, Carbon, 30 (1992) 995-1000. https://doi.org/10.1016/0008-6223(92)90127-i.

[7] L. Lahaye, P. Ehrburger, Fundamental issues in control of carbon gasification reactivity, Berlin: Springer Science & Business Media, 2012.

[8] S. Nomura, H. Ayukawa, H. Kitaguchi, T. Tahara, S. Matsuzaki, M. Naito, S. Koizumi, Y. Ogata, T. Nakayama, T. Abe, Improvement in blast furnace reaction efficiency through the use of highly reactive calcium rich coke, Isij International, 45 (2005) 316-324.

https://doi.org/10.2355/isijinternational.45.316.

[9] S. Nomura, M. Naito, K. Yamaguchi, Post-reaction strength of catalyst-added highly reactive coke, Isij International, 47 (2007) 831-839. https://doi.org/10.2355/isijinternational.47.831.

[10] K. Higuchi, S. Nomura, K. Kunitomo, H. Yokoyama, M. Naito, Enhancement of Low-temperature Gasification and Reduction by Using Iron-coke in Laboratory Scale Tests, Isij International, 51 (2011) 1308-1315. https://doi.org/10.2355/isijinternational.51.1308.

[11] H. Wang, M. Chu, Z. Wang, W. Zhao, Z. Liu, J. Tang, Z. Ying, Research on the post-reaction strength of iron coke hot briquette under different conditions, Jom, 70 (2018) 1929-1936. https://doi.org/10.1007/s11837-018-3036-4.

[12] H. Wang, W. Zhao, M. Chu, Z. Liu, J. Tang, Z. Ying, Effects of coal and iron ore blending on metallurgical properties of iron coke hot briquette, Powder Technology, 328 (2018) 318-328. https://doi.org/10.1016/j.powtec.2018.01.027.

[13] R. Xu, B. Dai, W. Wang, J. Schenk, Z. Xue, Effect of iron ore type on the thermal behaviour and kinetics of coal-iron ore briquettes during coking, Fuel Processing Technology, 173 (2018) 11-20. https://doi.org/10.1016/j.fuproc.2018.01.006.

[14] R. Xu, H. Zheng, W. Wang, J. Schenk, Z. Xue, Influence of iron minerals on the volume, strength, and CO_2 gasification of ferro-coke, Energy & Fuels, 32 (2018) 12118-12127. https://doi.org/10.1021/acs.energyfuels.8b02644.

[15] H. Zheng, W. Wang, R. Xu, R. Zan, J. Schenk, Z. Xue, Effect of the Particle Size of Iron Ore on the Pyrolysis Kinetic Behaviour of Coal-Iron Ore Briquettes, Energies, 11 (2018). https://doi.org/10.3390/en11102595.

[16] H. Wang, M. Chu, B. Guo, J. Bao, W. Zhao, Z. Liu, J. Tang, Investigation on Gasification Reaction Behavior and Kinetic Analysis of Iron Coke Hot Briquette under Isothermal Conditions,

Steel Research International, 90 (2019). https://doi.org/10.1002/srin.201800354.

[17] H. Wang, M. Chu, W. Zhao, Z. Liu, J. Tang, Influence of Iron Ore Addition on Metallurgical Reaction Behavior of Iron Coke Hot Briquette, Metallurgical and Materials Transactions B-Process Metallurgy and Materials Processing Science, 50 (2019) 324-336. https://doi.org/10.1007/s11663-018-1481-7.

[18] M.A. Diez, R. Alvarez, C. Barriocanal, Coal for metallurgical coke production: predictions of coke quality and future requirements for cokemaking, International Journal of Coal Geology, 50 (2002) 389-412. https://doi.org/10.1016/s0166-5162(02)00123-4.

[19] Q. Zhang, X.C. Wu, A.Z. Feng, M.R. Shi, Prediction of coke quality at Baosteel, Fuel Processing Technology, 86 (2004) 1-11. https://doi.org/10.1016/s0378-3820(03)00058-4.

[20] L. North, K. Blackmoreb, K. Nesbitt, M.R. Mahoney, Models of coke quality prediction and the relationships to input variables: A review, Fuel, 219 (2018) 446-466. https://doi.org/10.1016/j.fuel.2018.01.062.

[21] M.R. Khan, P.L. Walker, R.G. Jenkins, Swelling and plastic properties of coal devolatilized at elevated pressures of H_2 and He:influences of added iron-oxides, Fuel, 67 (1988) 693-699. https://doi.org/10.1016/0016-2361(88)90301-8.

[22] A. Uchida, Y. Yamazaki, K. Hiraki, T. Kanai, Y. Saito, H. Aoki, T. Inoue, N. Kikuchi, N. Okuyama, M. Hamaguchi, Evaluation of Properties of Hyper-coal with Iron Oxide Addition in Thermoplastic Range, Isij International, 53 (2013) 1165-1171. https://doi.org/10.2355/isijinternational.53.1165.

[23] R. Stanger, J. Borrowdale, N. Smith, W. Xei, T. Quang Anh, J. Lucas, T. Wall, Changes in Solvent-Extracted Matter for Heated Coal during Metaplast Formation Using High-Range Mass Spectrometry, Energy & Fuels, 29 (2015) 7101-7113. https://doi.org/10.1021/acs.energyfuels.5b01850.

[24] R. Stanger, T. Quang Anh, T. Attalla, N. Smith, J. Lucas, T. Wall, The pyrolysis behaviour of solvent extracted metaplast material from heated coal using LDI-TOF mass spectroscopy

measurements, Journal of Analytical and Applied Pyrolysis, 120 (2016) 258-268. https://doi.org/10.1016/j.jaap.2016.05.014.

[25] R. Stanger, T. Quang Anh, W. Xie, N. Smith, J. Lucas, J. Yu, E. Kennedy, M. Stockenhuber, T. Wall, The use of LDI-TOF imaging mass spectroscopy to study heated coal with a temperature gradient incorporating the plastic layer and semi-coke, Fuel, 165 (2016) 33-40. https://doi.org/10.1016/j.fuel.2015.10.028.

[26] S.X. Qiu, S.F. Zhang, Y. Wu, G.B. Qiu, C.G. Sun, Q.Y. Zhang, J. Dang, L.Y. Wen, M.L. Hu, J. Xu, R.J. Zhu, C.G. Bai, Structural transformation of fluid phase extracted from coal matrix during thermoplastic stage of coal pyrolysis, Fuel, 232 (2018) 374-383. https://doi.org/10.1016/j.fuel.2018.05.136.

[27] S.X. Qiu, S.F. Zhang, Q.Y. Zhang, G.B. Qiu, L.Y. Wen, Effects of iron compounds on pyrolysis behavior of coals and metallurgical properties of resultant cokes, Journal of Iron and Steel Research International, 24 (2017) 1169-1176. https://doi.org/10.1016/S1006-706X(18)30014-1.

[28] S.X. Qiu, S.F. Zhang, R.J. Zhu, Yue Wu, G.B. Qiu, J. Dang, L.Y. Wen, M.L. Hu, C.G. Bai, Influence of TiO_2 addition on the structure and metallurgical properties of coke, International Journal of Coal Preparation and Utilization, (2018). https://doi.org/10.1080/19392699.2018.1496913.

[29] S. Gupta, V. Sahajwalla, J. Burgo, P. Chaubal, T. Youmans, Carbon structure of coke at high temperatures and its influence on coke fines in blast furnace dust, Metallurgical and Materials Transactions B-Process Metallurgy and Materials Processing Science, 36 (2005) 385-394. https://doi.org/10.1007/s11663-005-0067-3.

[30] S. Gupta, D. French, R. Sakurovs, M. Grigore, H. Sun, T. Cham, T. Hilding, M. Hallin, B. Lindblom, V. Sahajwalla, Minerals and iron-making reactions in blast furnaces, Progress in Energy and Combustion Science, 34 (2008) 155-197. https://doi.org/10.1016/j.pecs.2007.04.001.

[31] S.X. Qiu, S.F. Zhang, Y.P. Fang, G.B. Qiu, C. Yin, R.G. Reddy, Q. Zhang, L.Y. Wen, Effects of poplar addition on tar formation during the co-pyrolysis of fat coal and poplar at high temperature, RSC Advances, 9 (2019) 28053-28060. https://doi.org/10.1039/c9ra03938d.

[32] F. Gayo, R. Garcia, M.A. Diez, Modelling the Gieseler fluidity of coking coals modified by multicomponent plastic wastes, Fuel, 165 (2016) 134-144. https://doi.org/10.1016/j.fuel.2015.10.053.

[33] T.P. Eskay, P.F. Britt, A.C. Buchanan, Pyrolysis of aromatic carboxylic acids: Potential involvement of anhydrides in retrograde reactions in low-rank coal, Energy & Fuels, 11 (1997) 1278-1287. https://doi.org/10.1021/ef9700745.

[34] F. Meng, S. Gupta, J. Yu, Y. Jiang, P. Koshy, C. Sorrell, Y. Shen, Effects of kaolinite addition on the thermoplastic behaviour of coking coal during low temperature pyrolysis, Fuel Process. Technol., 167 (2017) 502-510. https://doi.org/10.1016/j.fuproc.2017.08.005.

[35] K. Miura, K. Mae, W. Li, T. Kusakawa, F. Morozumi, A. Kumano, Estimation of hydrogen bond distribution in coal through the analysis bf OH stretching bands in diffuse reflectance infrared spectrum-measured by in-situ technique, Energy & Fuels, 15 (2001) 599-610. https://doi.org/10.1021/ef0001787.

[36] K. Miura, K. Mae, M. Shimada, H. Minami, Analysis of formation rates of sulfur-containing gases during the pyrolysis of various coals, Energy & Fuels, 15 (2001) 629-636. https://doi.org/10.1021/ef000185v.

[37] L. Shi, Q. Liu, X. Guo, W. Wu, Z. Liu, Pyrolysis behavior and bonding information of coal - A TGA study, Fuel Process. Technol., 108 (2013) 125-132. https://doi.org/10.1016/j.fuproc.2012.06.023.

[38] B. Tian, Y. Qiao, X. Lin, Y. Jiang, L. Xu, X. Ma, Y. Tian, Correlation between bond structures

554 and volatile composition of Jining bituminous coal during fast pyrolysis, Fuel Process. Technol.,
555 179 (2018) 99-107. https://doi.org/10.1016/j.fuproc.2018.06.019.
556 [39] B. Tian, Y.-y. Qiao, Y.-y. Tian, Q. Liu, Investigation on the effect of particle size and heating
557 rate on pyrolysis characteristics of a bituminous coal by TG-FTIR, Journal of Analytical and Applied
558 Pyrolysis, 121 (2016) 376-386. https://doi.org/10.1016/j.jaap.2016.08.020.
559 [40] A. Arenillas, C. Pevida, F. Rubiera, R. Garcia, J.J. Pis, Characterisation of model compounds
560 and a synthetic coal by TG/MS/FTIR to represent the pyrolysis behaviour of coal, Journal of
561 Analytical and Applied Pyrolysis, 71 (2004) 747-763. https://doi.org/10.1016/j.jaap.2003.10.005.
562 [41] Q. Liu, S. Wang, Y. Zheng, Z. Luo, K. Cen, Mechanism study of wood lignin pyrolysis by using
563 TG-FTIR analysis, Journal of Analytical and Applied Pyrolysis, 82 (2008) 170-177.
564 https://doi.org/10.1016/j.jaap.2008.03.007.
565 [42] S. Zhang, F. Zhu, C. Bai, L. Wen, C. Zou, Thermal behavior and kinetics of the pyrolysis of the
566 coal used in the COREX process, Journal of Analytical and Applied Pyrolysis, 104 (2013) 660-666.
567 https://doi.org/10.1016/j.jaap.2013.04.014.
568 [43] M.M. Maroto-Valer, C.J. Atkinson, R.R. Willmers, C.E. Snape, Characterization of partially
569 carbonized coals by solid-state C-13 NMR and optical microscopy, Energy & Fuels, 12 (1998) 833-
570 842. https://doi.org/10.1021/ef970196x.
571 [44] S. Nomura, K.M. Thomas, Fundamental aspects of coal structural changes in the thermoplastic
572 phase, Fuel, 77 (1998) 829-836. https://doi.org/10.1016/s0016-2361(97)00259-7.
573 [45] S. Lee, J. Yu, M. Mahoney, P. Tremain, B. Moghtaderi, A. Tahmasebi, R. Stanger, T. Wall, J.
574 Lucas, Study of chemical structure transition in the plastic layers sampled from a pilot-scale coke
575 oven using a thermogravimetric analyzer coupled with Fourier transform infrared spectrometer, Fuel,
576 242 (2019) 277-286. https://doi.org/10.1016/j.fuel.2019.01.024.

[46] Y. He, R. Zhao, L. Yan, Y. Bai, F. Li, The effect of low molecular weight compounds in coal on the formation of light aromatics during coal pyrolysis, Journal of Analytical and Applied Pyrolysis, 123 (2017) 49-55. https://doi.org/10.1016/j.jaap.2016.12.030.

[47] A.H. Tchapda, V. Krishnamoorthy, Y.D. Yeboah, S.V. Pisupati, Analysis of tars formed during co-pyrolysis of coal and biomass at high temperature in carbon dioxide atmosphere, Journal of Analytical and Applied Pyrolysis, 128 (2017) 379-396. https://doi.org/10.1016/j.jaap.2017.09.011.

[48] K. Miura, Mild conversion of coal for producing valuable chemicals, Fuel Process. Technol., 62 (2000) 119-135. https://doi.org/10.1016/s0378-3820(99)00123-x.

[49] J. Yu, J.A. Lucas, T.F. Wall, Formation of the structure of chars during devolatilization of pulverized coal and its thermoproperties: A review, Progress in Energy and Combustion Science, 33 (2007) 135-170. https://doi.org/10.1016/j.pecs.2006.07.003.

[50] K. I, I. S, M. T, Structure and thermoplasticity of coal, Nova publishers, 2005.